

Continental freshwater carbonate coated grains: oncoids in Quaternary deposits of the Serra da Bodoquena region, Central-West Brazil

Adelita Carolina Rodrigues^{1,2} , Larissa da Rocha Santos^{1,3} , Leonardo Fadel Cury¹ , Anelize Bahniuk Rumbelsperger¹ 

Abstract

Oncoid nucleation and growth have been attributed to microorganism activity, commonly cyanobacteria, resulting in the trapping of organic, bioclastic or lithoclastic nuclei by concentric laminations. However, the factors controlling these processes are not well understood, especially regarding freshwater precipitation systems. Freshwater oncoids from alluvial terraces underlying paludal tufas in Quaternary carbonate deposits in Central-West Brazil (Bodoquena downstream plains) were submitted to petrological studies by optical microscope, x-ray diffraction and fluorescence, scanning electron microscopy and C&O stable isotopes analyses. Biogenic structures where well-preserved cyanobacteria EPS sheath structures suggest *in vivo* precipitation by CO₂ concentrating mechanisms, whereas smooth rhomb calcite crystals likely indicate *post mortem* precipitation. The four identified morphologic features of spherical and subspherical oncoid types suggest growing in a shallow water body, with constant laminar flow and the absence of predators. The chemical and isotopic composition of the oncoids may represent nucleation and growth under relatively milder climatic conditions than today. This oncoid nucleation system may bring valuable information about climatic changes in Central-West Brazil (Tropical South Hemisphere) at the end of the Pleistocene and the beginning of the Holocene.

KEYWORDS: freshwater oncoids; continental carbonates; cyanobacteria calcification; microbial; EPS sheath structures.

INTRODUCTION

Oncoids are carbonate-coated grains produced by microorganism activity, commonly cyanobacteria, resulting in the trapping of organic, bioclastic, or lithoclastic nuclei by concentric laminations (Logan *et al.* 1964, Dahanayake 1978, Flügel 2010). Although the term 'oncoids' does not represent a genetic terminology, it is commonly used to refer to nodular coated grains formed by microbial activity (Flügel 2010).

As a microbialite and a carbonate coated grain, oncoids generally can bring palaeoclimatic and palaeoenvironmental information (Védrine *et al.* 2007, Zhang *et al.* 2015, Sequero *et al.* 2020) since they require specific factors for their full development, the most critical including:

- incidence of light that allows cyanobacterial colony growth, (Leinfelder and Hartkopf-Fröder 1990, Hägele *et al.* 2006);

- water body features such as depth, temperature, energy and low sedimentary input that enable nucleation and allow the development of a variety of morphologies and sizes (Logan *et al.* 1964, Riding 1975, Dahanayake 1978, Hägele *et al.* 2006, Védrine *et al.* 2007, Zhang *et al.* 2015);
- physicochemical conditions of the water and atmosphere that provide resources for cyanobacteria calcification, also predicting the oncoid framework (Merz 1992, Merz-Preiß and Riding 1999, Riding 2006, Sequero *et al.* 2020);
- lack of predators and competitive biota, enabling the oncoids' nucleation and growth in a free-competition/ predation environment (Riding and Awramik 2000, Hägele *et al.* 2006, Riding 2006).

This study focuses on cool freshwater oncoids, up to 10 mm long, found in the alluvial terraces of the Formoso River, Serra da Bodoquena region in Central-West Brazil. The aims of this work were:

- describing the oncoid occurrences in the alluvial terraces of the Formoso River;
- identifying the factors controlling their growth, with particular reference to microbial activity;
- understanding the oncoids' significance in the regional Quaternary carbonate deposits context, considering that oncoids have only been reported to occur stratigraphically below tufas (paludal and riverine).

¹Lamir Institute, Geology Department, Universidade Federal do Paraná – Curitiba (PR), Brazil. E-mails: adelita.carolina15@gmail.com, anelize.bahniuk@ufpr.br, lrsantos.geo@gmail.com, cury@ufpr.br, anelize.bahniuk@ufpr.br

²Graduate Program of Geology, Universidade Federal do Paraná – Curitiba (PR), Brazil.

³Postgraduate Program of Geology, Universidade Federal do Paraná – Curitiba (PR), Brazil.

*Corresponding author.



Through the evaluation of the main factors influencing the oncoïd nucleation and growth in the Serra da Bodoquena Region, we suggest an old nucleation context for those carbonate-coated particles that involves climatic changes in the southern hemisphere during the Quaternary Period.

BACKGROUND

Geological setting

The studied oncoïd occurrences are located at Serra da Bodoquena (21°15'S, 56°34'W), in the Paraguay Fold Belt, southwest of the Pantanal wetlands (Mato Grosso do Sul State, Brazil). The Serra da Bodoquena (Fig. 1) is a geomorphological domain constituted of a set of hills reaching elevation of 800 m, distributed over a 220 km long and 40 km wide N-S-trending structure, considered a carbonate plateau sustained by the Neoproterozoic metacarbonates, metapelites, and metapsammitic rocks of the Corumbá Group (Boggiani *et al.* 1993, Oliveira *et al.* 2017).

The Serra da Bodoquena is drained by several streams and creeks in which one example is the Formoso River and its

tributaries that drain the Eastern Bodoquena ridge. The rivers' freshwater dissolves the metacarbonate rocks of the Corumbá Group and forms a karstic system, providing the carbonatic source for the Quaternary carbonate precipitation on the downstream plains (Boggiani *et al.* 1993, Sallun Filho *et al.* 2009a, Oliveira *et al.* 2017).

The downstream Quaternary deposits are formed due to bicarbonate and calcium ion precipitation. However, they show many particularities involving biological activity and geomorphological relief features (Oste *et al.* 2021).

The tufa deposits along the Formoso river are proposed to be included in the Pleistocene-Holocene *Serra da Bodoquena Formation* (Sallun Filho *et al.* 2009a), (Fig. 1) and it is subdivided into two members: *Rio Formoso* (riverine tufas) and *Fazenda São Geraldo* (paludal tufas) members. The Rio Formoso Member includes both active and inactive riverine tufa deposits (Sallun Filho *et al.* 2009a).

- The paludal tufas consist of friable micrite deposits occurring on river banks (Boggiani *et al.* 2002), possibly formed in oxbow lakes (Boggiani *et al.* 2002, Utida *et al.* 2017) of 6,530 to 6,310 yr BP age (^{14}C , 21°15'S, 56°34'W) (Sallun Filho *et al.* 2009b);

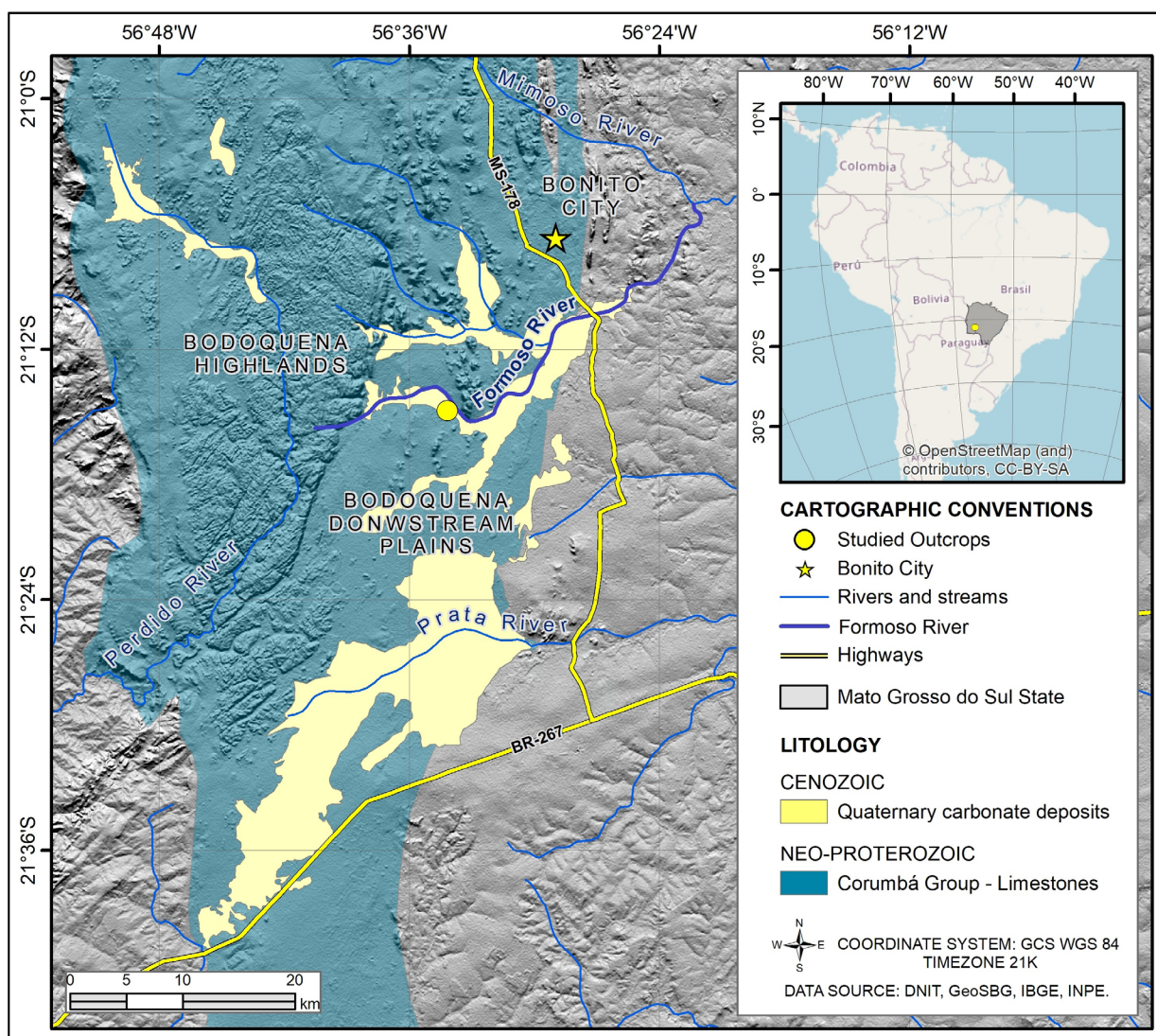


Figure 1. A. Geological context and location of the studied outcrops near Serra da Bodoquena Highlands.

- The riverine tufa deposits occur in dams and waterfall settings, where the inactive tufa provided ages from 2,130 to 3,410 yr BP (^{14}C , 21°02'S, 56°51'W) (Sallun Filho *et al.* 2009b), forming stratified deposits recording the annual deposition cycle, with increasing growth in warm and rainy periods and decrease or absence of growth during cold periods (Boggiani *et al.* 2002, Sallun Filho *et al.* 2009a, Oliveira *et al.* 2017).

The active and inactive tufas are porous, displaying a wide range of structures related to macrophyte growth (mainly bryophytes) and microorganisms. The main facies are described as stromatolitic and phytoherm boundstone, phytoclastic rudstones, as well as oncoidal grainstones and rudstones (Oliveira *et al.* 2017, Oste *et al.* 2021).

The Serra da Bodoquena region is located in Tropical South America, commonly referred as the atmosphere's 'walker' circulation zone (Baker *et al.* 2001). The region is considered the most sensitive to atmospheric variation and important for paleoclimatic reconstruction using oxygen isotope record (‰ , V-PDB, V-SMOW) correlated to insolation (W m^{-2}) in U/Th dated samples (Baker *et al.* 2001, Wang *et al.* 2004, Cruz Jr. *et al.* 2005, Seltzer *et al.* 2014, Novello *et al.* 2019) while using a pollen sedimentary record (Absy *et al.* 1991, Ledru 1993, Whitney *et al.* 2011).

Cyanobacteria related to oncoids

The cyanobacteria are wrapped in a biofilm known as EPS (protective extracellular polymeric substance) (Riding and Awramik 2000, Decho *et al.* 2005, Riding 2006) that is able to catalyze calcium carbonate (CaCO_3) precipitation (Decho *et al.* 2005, Dupraz and Visscher 2005, Dupraz *et al.* 2009).

The cyanobacteria colonization coupled with calcium carbonate precipitation might form concentric laminations around a lithoclastic or bioclastic nuclei resulting in a carbonate-coated grain (Logan *et al.* 1964, Dahanayake 1978).

Considering that carbonate precipitation and its mediation by biological activity are the core of oncoid nucleation and growth, the ecosystem present in the freshwater coated grains or oncoids are suitable for a series of environmental paleoclimatic interpretations.

Under this classification, the coated grains described as oncoids were previously interpreted as related to organisms from Nostocales order (*Rivularia*, *Calothrix*, *Schizothrix*, *Phormidium*) (Riding 1975, Pentecost 1978, Pentecost and Talling 1987, Hägele *et al.* 2006). In particular, the *Rivularia* genera was considered a bioindicator or environmental proxy since its proliferation is generally restricted to specific physical-chemical parameters (Perona and Mateo 2006, Berrendero *et al.* 2008, Oren 2015, Shalygin *et al.* 2018), even being reported in a series of ecological niches as freshwater, terrestrial, and marine environments (Berrendero *et al.* 2008).

METHODS

The studied oncoids were collected in the Formoso river alluvial terraces (GCS WGS84: Longitude 56°3', Latitude

21°1'), occurring as rudstones and floatstones, overlaid by the paludal tufas (Fig. 2).

Four oncoids that represent each morphology type and one well-cemented floatstone were selected for petrographic studies in thin sections using the Zeiss Stereo microscopic model at Lamir Institute (LAMIR at the Federal University of Parana), and an Olympus BX51 at CTAF Institute (*Centro de Tecnologias Avançadas em Fluorescência* — Biology Department, Universidade Federal do Paraná). The sample descriptions followed the Dunham limestone classification (1962) modified by Embry and Klovan (1971), and the coated grains' classification followed Flügel (2010) descriptive terminology (Dunham 1962, Embry and Klovan 1971, Flügel 2010).

To evaluate the presence of biological activity and to describe the oncoids' internal laminations, scanning electron microscopic (SEM) analyses were conducted using a JEOL SEM model 6010LA, equipped with an energy dispersive X-ray spectrometer. One lithified rudstone, and six oncoidal fragments representative of morphology types and nuclei composition were Au-coated before the SEM examination, and the analyses were conducted with an accelerating voltage of 20 kV using the minimum beam diameter. In addition, three morphology representative samples were selected to be evaluated in a SEM TESCAN VEGA 3 LMU, EDS type chemical analysis system (Oxford) using the AZ Tech software (Advanced) with 80 mm² SDD type detector.

Mineralogical and geochemical analyses were carried out at LAMIR with five total powdered samples (325 to 400 mesh), three oncoidal samples, and two lithified rudstones. The mineralogical composition was determined using X-ray diffraction (XRD) through a PANalytical diffractometer, Empyrean model with an X-accelerator detector, equipped with a Cu tube. Scans from bulk samples were run from 2 θ angles from 3 to 70°, using a step-size of 0.016° and count time of 10.16 s per step. The chemical composition (wt%) of the main oxides (CaO , MgO , SiO_2 , Al_2O_3 , Fe_2O_3 , Na_2O , K_2O , TiO_2 , MnO , and P_2O_5) and four trace elements (Sr, Ba, S, and Cl) were obtained via quantitative X-ray fluorescence through a PANalytical model Axiom-Max with Rh tube, using a lithium tetraborate fused bead.

C and O stable isotopes were conducted in a Gas Bench II and a Thermo Delta V Advantage mass spectrometer (ThermoFisher Scientific) using 400 to 600 μg samples, digested with orthophosphoric acid at 72°C with. The results were referenced to the V-PDB scale using the following reference materials: NBS 19, IAEA-CO-1, IAEA-CO-8, and IAEA-CO-9. Standard deviation was reported (1σ) to the internal deviation of 8 to 10 readings of the same preparation.

RESULTS

Facies description

The studied deposits were described as fluvial terraces that flank the actual fluvial floodplain and the Formoso River's current stream, and the five main facies described were (Fig. 2): A basal layer of siliciclastic clay (Claystones) and four allochthonous calcareous facies that consist of oncoidal

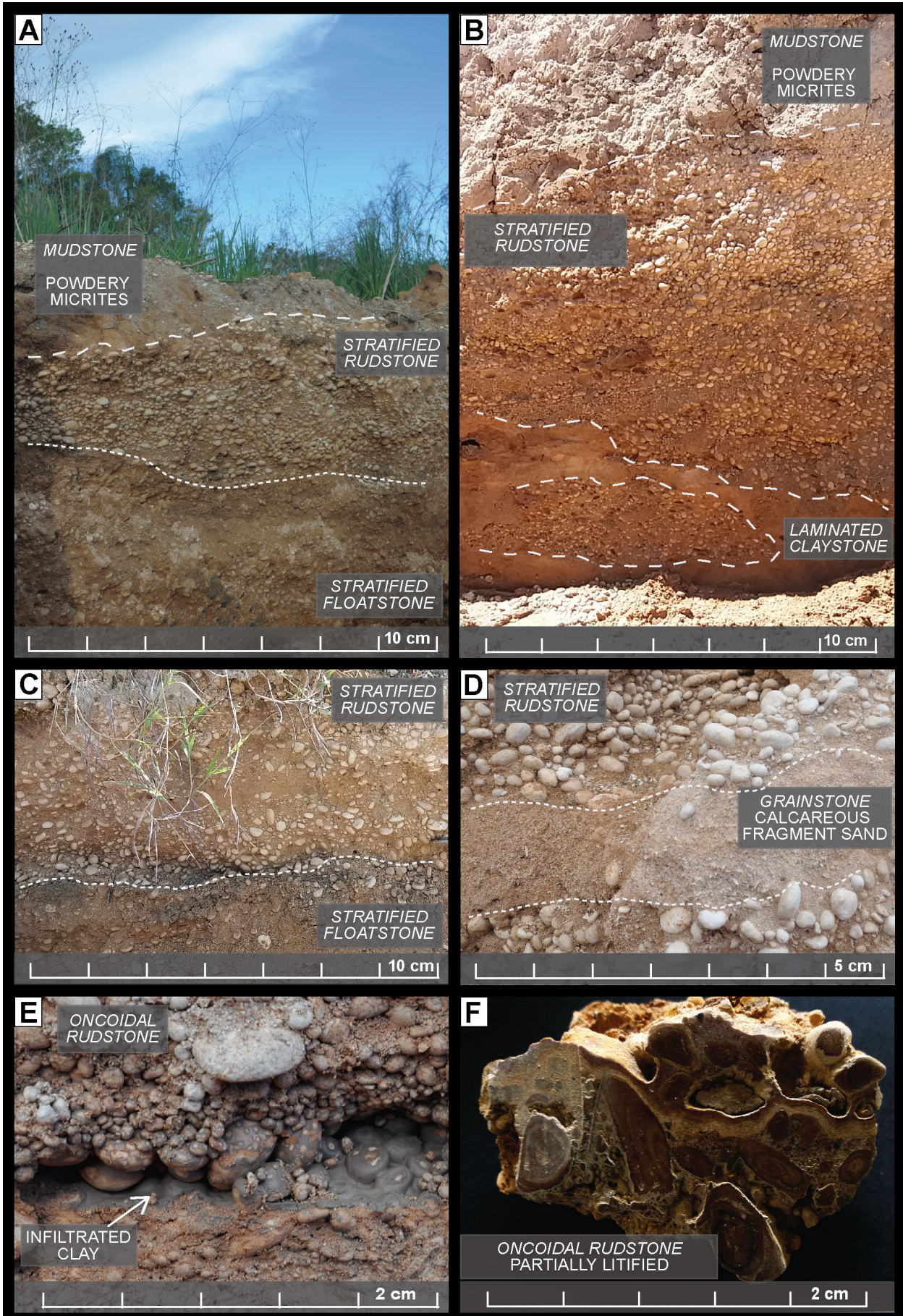


Figure 2. Outcrop view of the Formoso River alluvial terraces; (A) Rudstones (Rs) and floatstones (Fs) showing imbricated oncolite in a lateral view of trough cross-stratification, the massive mudstone (Mm) overlies the oncolite lenses; (B) Stratified rudstones (Rs), massive mudstones (Mm), and laminated Claystone (Cl) at the base; (C) Lenticular grainstone (Gl), composed of biogenic calcareous fragments in sand fraction, predominantly algae or macrophytes tubes, stalks and Mollusca shells; (D) Rudstones (Rs) and Floatstones (Fs) and their transitional contact (dashed line); (E) Oncoidal Rudstone lenses with infiltrated clay; (F) Transversal cut of oncolite hand-sample showing a bimodal distribution of the framework oncoids and early cementation features, found in small occurrences.

lenses (Rudstones and Floatstones), calcareous sand lenses (Grainstones), and at the top occur a powdery micrites layer (Mudstones), as detailed below.

Claystone facies — laminated clay (Cl)

The massive to crudely laminated brown claystones in the studied terrace correspond to its basal interval with 0.5 to 1.5 m-thick, and up to 10m wide observed (Fig. 2B). The claystone has a poor plastic aspect and stratification is visible. Organic components such as carbonaceous fragments occur in smaller proportions (5%). Oncoids with diameters < 2 mm were observed, dispersed at the upper part of the clay layers.

Calcareous sand — stratified grainstone (Gs)

The Gs facies occur in 10 to 30 cm-thick highly friable lenses of biogenic carbonate fragments. The framework grain sizes range between 0,5 to 2 mm, and fragments with 2 to 16 mm are make up 20% of the sample. The main composition is represented by calcified tubes of calcareous algae, stalks of macrophytes, calcified Mollusc shells, oncoids, and partially nucleated oncoidal fragments (Fig. 2D). The colors are whitish to yellowish.

Oncoidal lenses — stratified rudstones and floatstones (Rs and Fs)

The oncoidal facies occurs as 0.5 to 1.5 m-thick up to 10 m wide highly friable lenses. The framework is constituted of oncoids ranging from 0,5 mm to 6 cm, forming oncoidal rudstones and floatstones with medium-sized (up to 3 m) through cross-stratification (Figs. 2A, 2B and 2C). The oncoids' sizes range from 0.5 to 6 cm on the x-axis (longest length) up to 3 cm on the y axis (height). The z-axis, although variable, occurs with less thickness or the same size as the x-axis size.

The rudstones and floatstones' matrix is comprised of bioclasts or limestone fragments in a sand fraction such as shells, calcified tubes of calcareous algae, smaller oncoids, or oncoidal fragments smaller than 2 mm. Quartz grains partially encrusted with calcium carbonate are also common and the Floatstone matrix may also include clay. The proportions of brown clay are greater at the base of outcrops, gradually disappearing to the top. The rudstone facies are absent in clay.

In the stratified rudstone (Rs) facies lenses with infiltrated gray clay (Fig. 2E), of high plasticity occur. In the stratified floatstone (Fs) facies occurs a well-lithified layer around 10 to 30 cm- thick and 1 m wide (Fig. 2F).

Mudstone facies — powdery micrites/massive mudstone (Mm)

The Mm facies overlies the oncoidal facies (Figs. 2A and 2B), and it is composed of gray powdery micrites and calcareous fragments (< 10%) such as calcified Mollusc shells, calcareous algae tubes and macrophytes stalks. The Mm facies overlie the oncolytic facies through an abrupt contact. The Mm facies are highly friable with a massive structure, where Cyanobacteria filaments are encrusted with carbonate crystals.

Oncoids morphologic features

The oncoids were classified based on their shapes into four main types (Fig. 3):

- shape 1: includes oncoids showing triangular shapes, with concave tops, elliptical sides and no laminations at the base (Fig. 3A);
- shape 2: oncoids with triangular shapes and concave tops, thinner laminations on the base compared to top and side laminations (Fig. 3B);
- shape 3: oncoids with an elliptical shape and continuous laminations of similar thickness (Fig. 3C);
- shape 4: oncoids with spherical shapes, continuous and similar thick-sized laminations (Fig. 3D).

Petrographic features

Three internal structural patterns were distinguished in the studied oncoids (Fig. 4):

- massive micrite lamination with moldic porosity (Fig. 4A);
- bacterial shrub structure (Fig. 4A);
- layers with amorphous organic matter between laminations (Fig. 4B).

Their nuclei consist of sub-angular to sub-rounded (Fig. 4C), low to medium sphericity quartz grains (Fig. 4D), moldic microorganisms (Fig. 4E), moldic Mollusca shells including Bivalve and Gastropod Groups, as well as amorphous silica replacing relict nuclei (Fig. 4F). Early diagenetic features include mosaic calcite cement and microcrystalline iron oxides and hydroxides cement.

The oncoids also show continuous or discontinuous growth phases, sometimes with remnant oncoids eroded (Fig. 4G) as a new nucleus-substrate to a subsequent growing phase (Fig. 4H).

Oncoid microfacies

Massive micrite with moldic porosity

The massive micrite layers (Fig. 5) represent the main microfacies forming 100 to 400 μm -thick layers around the nucleus (Fig. 5A). The EPS sheath relict structures related to the cyanobacteria filaments occur throughout the lamination (Fig. 5B). The filament structures show $\sim 6 \mu\text{m}$ in diameter and lengths of 50 to 250 μm (Fig 5C). The related moldic porosity represents up to 7% of the sample. Smooth rhomb calcite crystals are also common (Fig. 5D), usually around $> 20 \mu\text{m}$, surrounded by subhedral crystal aggregates (Fig. 5E). Rare cyanobacteria calcified filaments (Fig. 5F), up to $3 \mu\text{m}$ in diameter, are observed in the massive micrite layers (Fig. 5G). Needle calcite crystals up to $2 \mu\text{m}$ complete this textural pattern (Fig. 5H).

Bacterial shrub

The bacterial shrub structure forms discontinuous lamination (Fig. 6) and is usually responsible for irregularities in the oncoid shapes. When the bacterial shrub is well developed (0.5 to 1.5 cm), there is a growth predominance on one side of the oncoid per growing cycle (Figs. 6A and 6B).

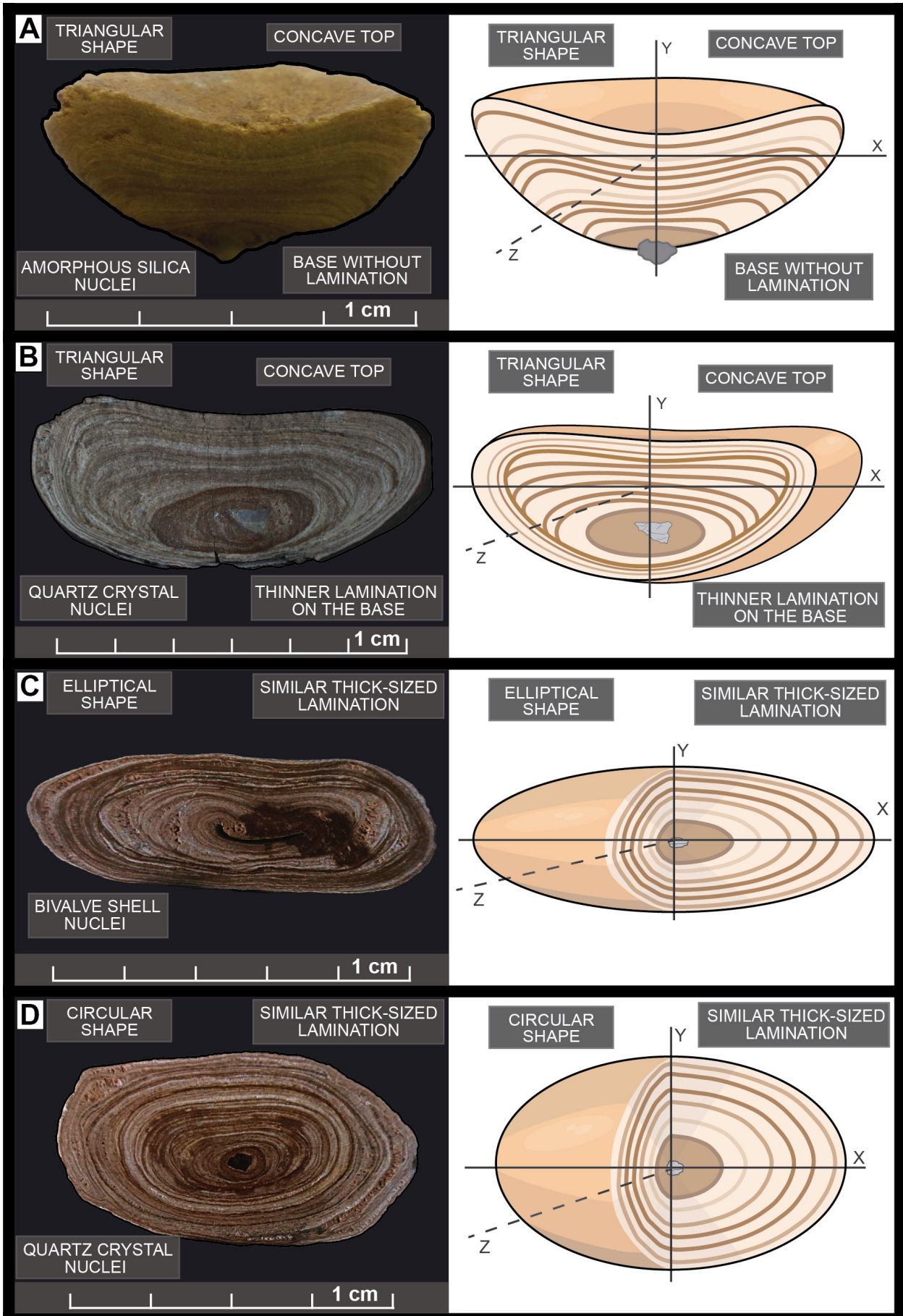


Figure 3. Oncoids' morphologic features. (A) Type 1, triangular, showing no laminations at the base or the concave top; (B) Type 2, triangular, showing a concave top and thin basal laminations; (C) Type 3, with elliptical shape, regular, continuous, and similar thick-sized laminations, slightly thicker at the sides; (D) Type 4, showing spherical shape, regular, continuous, and similar thick-sized laminations. Nucleus not used to indicate morphologic features; (A) Amorphous silicon nuclei; (B) Quartz crystal nuclei; (C) Moldic shell nuclei; (D) Quartz crystal nuclei.

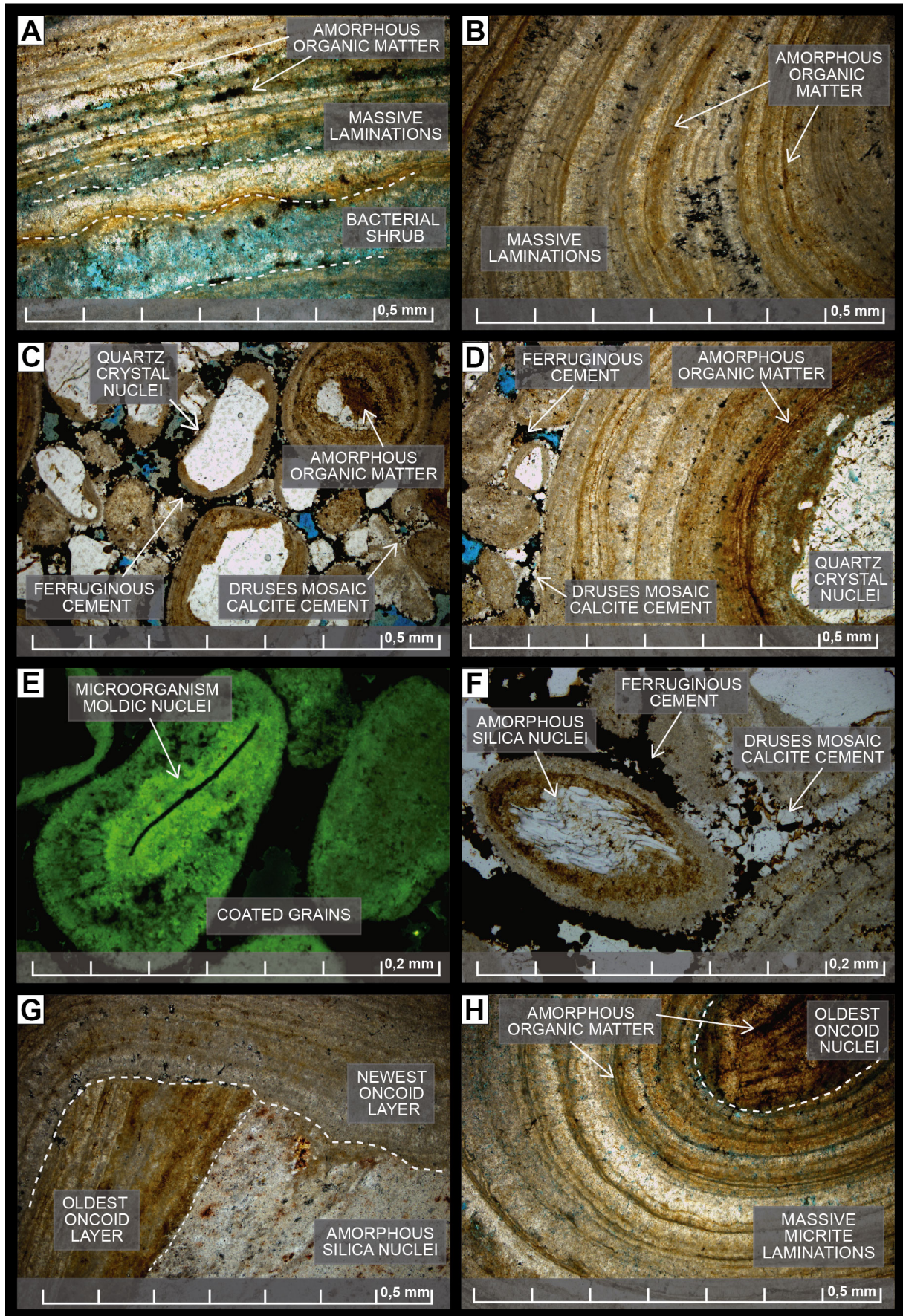


Figure 4. Examples of the main petrographic aspects of the studied oncooids (A, B, C, D, F, G, H) under natural light and (E) UV epifluorescence. (A) Alternating lamination cycles with massive and bacterial shrub laminations, porosity filled by amorphous organic matter; (B) Carbonate massive and concentric laminations, porosity filled by amorphous organic matter; (C) Carbonate coated grains with quartz crystal nucleus, early diagenesis features such as druses mosaic calcite, ferruginous cement; (D) Oncooids with carbonate concentric lamination around a quartz crystal nucleus, early diagenesis features such as druses mosaic calcite and ferruginous cement; (E) Carbonate coated grains, detail for microorganism moldic porosity; (F) Carbonate coated grains with amorphous silica nuclei, early diagenesis features such as druses mosaic calcite and ferruginous cement; (G) Carbonate massive and concentric laminations around the oldest oncoid nuclei, porosity filled by amorphous organic matter; (H) Oncoid with more than one nucleation stages, amorphous silica substituting relict nuclei.

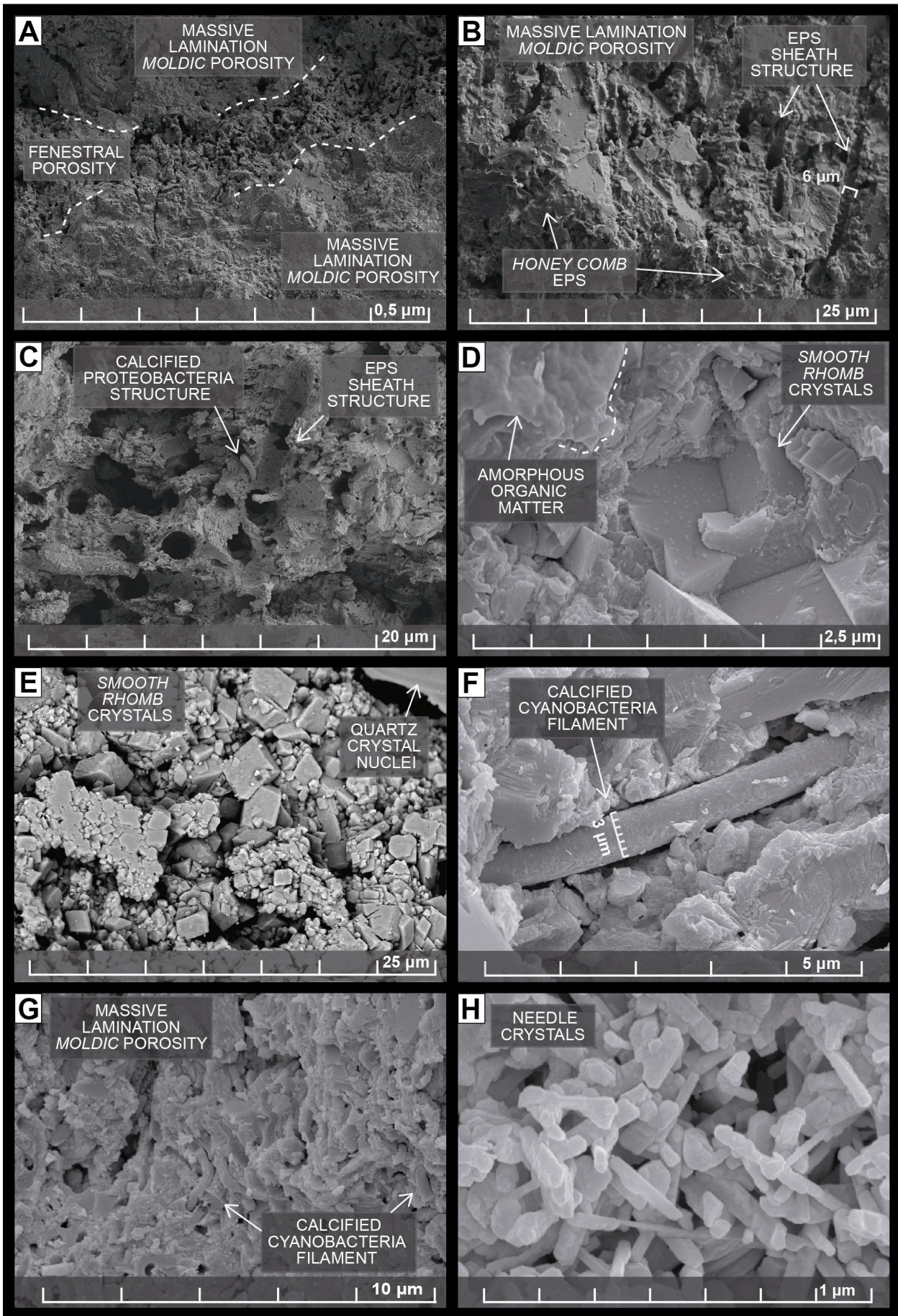


Figure 5. Massive micrite with *moldic* porosity. SEM photomicrograph. (A) Massive micrite layers showing highly porous layers with moldic porosity; (B) Massive lamination with *moldic* porosity by EPS sheath structure cyanobacteria filamentous and *honeycomb* EPS; (C) *Moldic* porosity of EPS sheath structure cyanobacteria filamentous with calcified proteobacteria structure; (D) Clusters of calcite *needle* crystals; (E) *Smooth rhomb* crystals next to a quartz crystal nucleus; (F) *Smooth rhomb* crystals and amorphous organic matter; (G) Massive lamination with *moldic* porosity and calcified cyanobacteria filament; (H) Massive lamination with calcified cyanobacteria filament.

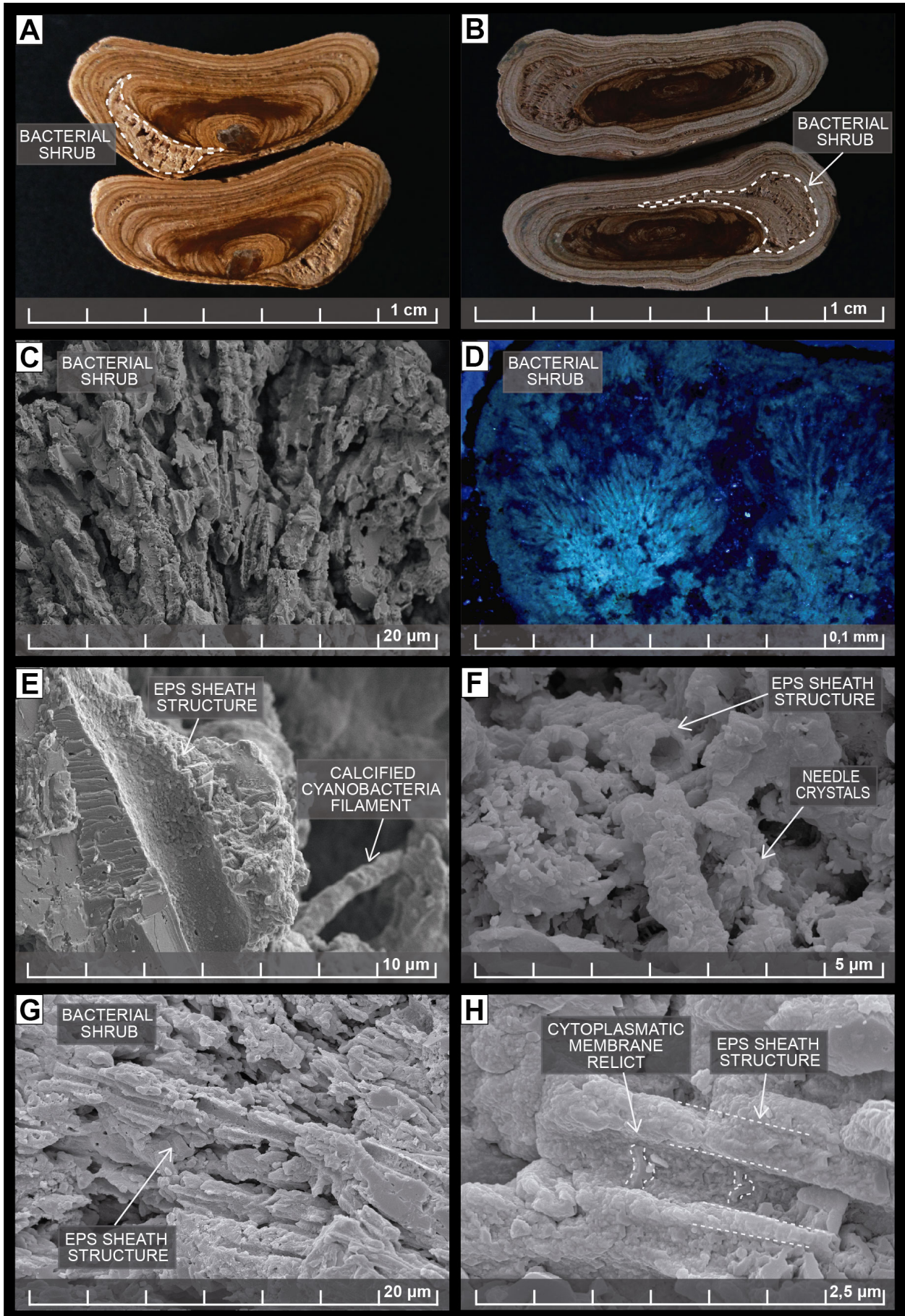


Figure 6. SEM photomicrograph and UV epifluorescence (D) of bacterial shrub structure. (A) Type 2 oncoïd with bacterial shrub areas; (B) Type 3 oncoïd with bacterial shrub areas; (C) Bacterial shrub structures; (D) Cyanobacteria arrangements in a bacterial shrub structure; (E) Filamentous cyanobacteria EPS sheath structure, and calcified cyanobacteria filament; (F) Filamentous cyanobacteria EPS sheath structure, and calcite *needle* crystals composite; (G) Filamentous cyanobacteria EPS sheath structure; (H) Detail of the relict cytoplasmic membrane within EPS sheath structure.

The calcite crystals show > 10 µm euhedral shapes, sparse cyanobacteria calcified filaments (Fig. 6E), and needle calcite crystals (Fig. 6F). Moldic porosity can reach 18% of the sample with ~ 100 µm in length (Fig. 6G) 6 µm-diameter pores (Fig. 6H).

Microbial activity related structures summary

Four major types of calcite crystal structures that compound the microfacies can be described as:

- EPS sheath structure: represents specifically a calcification of the EPS sheath, without a filament preserved, occurring in both microfacies, in massive micrite as a moldic porosity and Bacterial Shrub as a tubular structure with a radial arrangement, showing a regular growth pattern on samples;
- Smooth Rhomb Crystals: represents rhombohedral crystal, occurring frequently in both microfacies and also showing a regular growth pattern along with the samples;
- Needle Crystals: observed normally in small clusters, rarely occurring without a regular pattern;
- Calcified filaments: in this situation, the filament is properly calcified without specific relation to the EPS sheath and does not form calcite structures. They rarely occur without a regular pattern.

Chemical and mineralogical composition

The energy-dispersive X-ray spectroscopy showed the main composition of Ca, O, and C, (5,000 to 12,000 cps) while Si, Al, K, and Fe occur in low proportions (> 1,000 cps) (For further detail, see supplementary material). The amorphous organic matter (Figs. 7A and 7B) occurs either in the moldic porosity (Figs. 7C and 7D) or disseminated throughout the lamination. The subsequent micrite-growth cycles trap the organic material (Figs. 7E–7H) and the later organic matter infiltrations represent a subordinate occurrence.

The bulk mineralogical composition of oncoids consists mainly of calcite and quartz, and it is similar in all studied oncoid morphology types. The bulk rock chemical composition shows CaO contents around 54%, SiO₂ from 0.77 to 1.35%, as well as minor Fe₂O₃, Al₂O₃, and MgO (Tab. 1).

Carbon and oxygen stable isotopes

Carbon and Oxygen stable isotopes (δ ‰VPDB) were investigated in oncoids (from *Rs* and *Fs*), calcareous fragments (*Gs*), and clays (*Cl*), representing the main facies described above (Tab. 2). Bulk rock oncoid samples (*Rs* and *Fs*) showed isotopic ratios between -5.55 to -6.13 ‰VPDB for δ¹³C and -7.37 to -7.51 ‰VPDB for δ¹⁸O. The calcareous fragments (*Gl*) showed relatively more negative δ¹³C ratios around -6.33 to -6.46 ‰VPDB. However, δ¹⁸O are similar, ranging from -7.41 to -7.82 ‰VPDB. Dissimilar ratios were observed in clays (*Cl*), where the values ranged from -3.96 to -6.62 ‰VPDB for δ¹³C, and -8.18 to -9.02 ‰VPDB for δ¹⁸O.

DISCUSSION

Oncoids nucleation, growth and morphology

The nucleation and growth of the oncoids start when the EPS allows microbial communities to attach themselves to the substrate (Decho *et al.* 2005, Decho and Gutierrez 2017). Several surfaces have the substrate potential to trigger nucleation, such as quartz grains or Mollusca shells. Therefore, the lamination is evidence of the oncoidal growth processes, with an interbedding of bacterial activity-related structures and pores filled with amorphous organic matter.

Studies of the *Rivularia haematites* have shown evidence of increased productivity during Winter and poorly calcified layers during Summer (Pentecost 1978, Pentecost and Talling 1987). Considering that Rivulariaceae and Nostocaceae families are the most common oncoid-forming microorganisms (Riding 1975, Pentecost 1978, Pentecost and Talling 1987, Leinfelder and Hartkopf-Fröder 1990, Riding and Awramik 2000, Hägele *et al.*, 2006, Shalygin *et al.* 2018), and by morphology comparison through SEM results (Reviere 2002, Shalygin *et al.* 2018) we interpreted that the EPS sheath structures may have originated from organisms of the Rivulariaceae family, whereas the calcified filamentous structures may be related to the Nostocaceae family.

The set of laminations are responsible for the oncoidal morphology, which has been used for environmental interpretation since they are able to provide water-energy conditions (Logan *et al.* 1964, Dahanayake 1978, Leinfelder and Hartkopf-Fröder 1990) and light incidence information (Leinfelder and Hartkopf-Fröder 1990, Hägele *et al.* 2006).

The genesis of concentric oncoids was initially interpreted as a result of rolling of the particles in submerged environments with constant movement, leading to the spheroid rounded shapes (Logan *et al.* 1964, Dahanayake 1978, Flügel 2010). However, new studies have suggested that spherical and subspherical oncoids may have *in situ* growth, with similar-thick lamination patterns, where coarse-grained substrates enhance growth in response to light reflection at the base of the oncoids, in which agitated hydraulic conditions are not a requirement (Leinfelder and Hartkopf-Fröder 1990, Hägele *et al.* 2006, Zhang *et al.* 2015).

Studies on oncoids of the Alz river in Germany suggested that differences in light incidence may cause eccentricity of the concentric lamination and the lack of mechanical disturbances and bearing allow *in situ* growing processes (Hägele *et al.* 2006). The described oncoid types have similar features to the ones described in the Alz river, such as different sizes of lamination causing oncoidal eccentricity (Fig. 8). Furthermore, the type 1 oncoid (concave top lacking basal lamination) does not bear evidence such as surface erosion and was likely attached to the substrate during growth. The *in-situ* growth implies the absence of carbonate production at the oncoid's base and may be indicative of either absence or reduced light incidence.

Type 2 may indicate that the initial oncoid nucleation stage occurred attached to the substrate and it was later detached. This process requires biofilm development and represents a

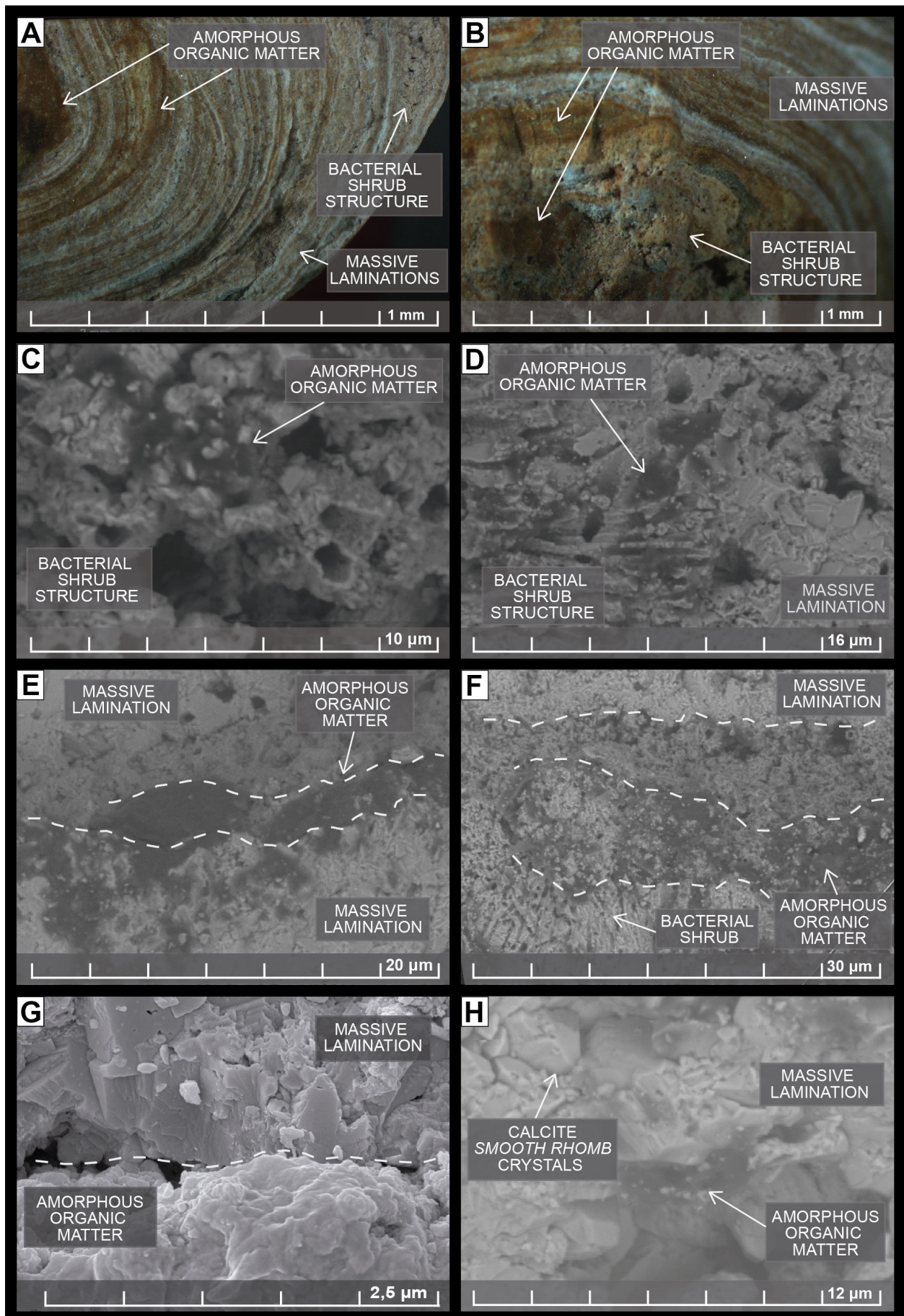


Figure 7. (A-B) Photomicrographs and SEM images of amorphous organic matter. (A) Type 2 oncoïd, with an amorphous organic matter concentration near to the oncoïd nuclei. Layers of organic matter also occur between massive micrite layers; (B) Type 2 oncoïd, showing bacterial shrub structure around the nuclei with the amorphous organic matter between massive micrite layers; (C and D) Amorphous organic matter in bacterial shrub structure; (E) Amorphous organic matter disseminated in massive micrite layers; (F) Amorphous organic matter disseminated in the transition between massive and bacterial shrub layering; (G) Amorphous organic matter trapped by massive lamination; (H) Amorphous organic matter filling pores in massive micrite layers with *smooth rhomb* calcite crystals.

Table 1. Major element distribution in Formoso River oncoids. Values in weight % oxides.

SAMPLE	CaO	MgO	SiO ₂	Al ₂ O ₃	Fe ₂ O ₃	K ₂ O	SrO	TiO ₂	MnO	P ₂ O ₅	LOI	SUM
Floatstone 01	31.73	0.16	33.21	2.42	3.69	0.13	0.04	0.14	0.57	0.04	27.87	100.01
Floatstone 02	43.72	0.11	13.76	0.68	4.31	0.03	0.05	0.04	0.71	0.03	36.20	99.66
Oncoid 03	54.05	0.13	0.77	0.35	0.75	0.02	0.06	0.03	0.18	0.03	43.63	99.99
Oncoid 04	53.68	0.08	1.35	0.41	0.29	0.02	0.06	0.03	0.04	0.02	43.99	99.96
Oncoid 05	54.06	0.07	0.99	0.42	0.40	0.02	0.07	0.03	0.04	0.02	43.61	99.73

Table 2. Carbon and oxygen stable isotopes ratios. Values in ‰VPDB.

Code	Sample	Facies	δ ¹³ C	1σ [δ ¹³ C]	δ ¹⁸ O	1σ [δ ¹⁸ O]
133/19-01	Claystone	Cl	-4.58	0.09	-9.02	0.05
133/19-09	Grainstone	Gl	-6.46	0.02	-7.82	0.09
133/19-11	Floatstone	Fs	-6.44	0.02	-7.57	0.06
133/19-12	Rudstone	Rs	-6.13	0.02	-7.44	0.09
133/19-13	Rudstone	Rs	-6.22	0.09	-7.41	0.04
133/19-16	Mudstone	Mm	-6.62	0.08	-8.8	0.05
133/19-22	Grainstone	Gl	-6.33	0.07	-7.54	0.05
133/19-23	Rudstone	Rs	-6.38	0.05	-7.41	0.04
133/19-33	Floatstone	Fs	-1.44	0.04	-7.56	0.04
133/19-35	Floatstone	Fs	-3.96	0.06	-8.18	0.05
133/19-44	Oncoid	Rs	-5.82	0.05	-7.51	0.06
133/19-45	Oncoid	Rs	-6.04	0.04	-7.39	0.05
195/18-01	Oncoid	—	-5.97	0.04	-7.66	0.05
195/18-02	Oncoid	—	-5.65	0.07	-7.53	0.07
195/18-03	Oncoid	—	-5.55	0.02	-7.37	0.03
195/18-04	Oncoid	—	-5.98	0.03	-7.44	0.04
195/18-05	Oncoid	—	-5.66	0.03	-7.39	0.03

transition between non-concentric laminations development to fully concentric ones.

The oncoids with spherical shapes (types 3 and 4) show concentric and similar thick size lamination. This pattern suggests oncoidal growth detached from the substrate, where the concentric biofilm may indicate a similar incidence of light around the oncoid, implying bearing occurrences.

Since most oncoids were nucleated around quartz grains of 0.1 to 1 mm, and considering the nucleation likely occurs below the deposition curve (Hjülstrom diagram), suggesting a flow velocity between 0.1 and 1 cm.s⁻¹. For oncoids nucleated from grains transported as bedload, the flow velocity would be between 1 to 20 cm.s⁻¹ (Nichols 2009).

Given the predominance of regular lamination in terms of format, continuity and linearity, oncoid genesis possibly occurs under a laminar flow influence. For oncoids nucleated on detrital quartz grains, only in initial nucleation stages, an estimate using the Reynolds number was proposed to infer the flow type, considering the water viscosity to be 1x10⁻³ Pa.s, the fluid specific mass 1.0 kg.m⁻³, the flow velocity of 0.1 to 1 cm.s⁻¹ (Hjülstrom diagram), and assuming that a laminar flow requires Re < 500, the water body depth could not exceed 50 cm to maintain a laminar flow (Nichols 2009).

Carbon and oxygen isotopic record and significance

Isotopic C and O ratios (δ ‰VPDB) in riverine and paludal tufas are controlled by karst groundwater (Andrews *et al.* 2000, Andrews 2006). At Central-West Brazil latitude (21°S), we can consider a similar δ¹⁸O to the ground and meteoric water (Gat 1971, Darling 2004) in the current climate, where continentality is the main factor that leads to relatively more negative δ¹⁸O values in the region (Garnett *et al.* 2006).

The δ¹⁸O ratios of -7.30‰ to -8.00‰ in the studied oncoids (Tab. 2) are close to results obtained in recent and sub-recent tufas of the Formoso River (Taika and Mimosa sites) in which the values range from -6.50‰ up to -8.50‰ (Oste 2017). This resembling results for ancient and recent tufa in comparison to oncoids, endorse the meteorological water source.

Regarding the stable carbon isotopes (δ ‰VPDB), it is mandatory to consider the degassing effect in tufas, where this continuous process might increase δ¹³C dissolved inorganic carbon (DIC) values, and consequently, influence the carbon isotopic values for tufas downstream (Pentecost and Spiro 1990). The photosynthesis effects controlled by cyanobacterial action remove the ¹²CO₂, resulting in the calcite ¹³C enrichment (Pentecost and Spiro 1990, Arp *et al.* 2001a, Arp *et al.* 2001b).

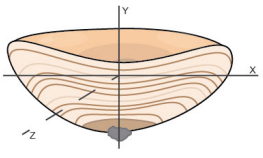
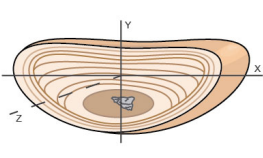
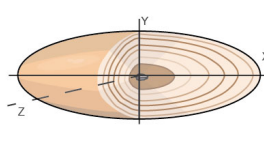
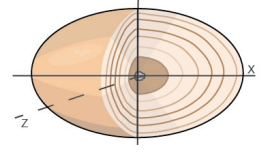
CONCAVE TOP ONCOIDS		SPHERICAL SHAPE ONCOIDS	
TYPE 1	TYPE 2	TYPE 3	TYPE 4
			
SITUATION A	SITUATION AB	SITUATION B	
NON CONCENTRIC LAMINATIONS	TRANSITION	TOTALLY CONCENTRIC LAMINATIONS	
WITHOUT CARBONATIC PRODUCTION AT THE BASE	REDUCED CARBONATIC PRODUCTION AT THE BASE	SIMILAR CARBONATIC PRODUCTION AROUND THE ONCOID	
<i>IN SITU</i> GROWTH	PARTIALLY <i>IN SITU</i> GROWTH	OFTEN SUBJECTED TO BEARING	
PROBABLY ATTACHED TO THE SUBSTRATE	PARTIALLY ATTACHED TO THE SUBSTRATE	PROBABLY DETACHED FROM THE SUBSTRATE	
ABSENCE OF LIGHT AT THE BASE	REDUCED INCIDENCE OF LIGHT AT THE BASE	SIMILAR INCIDENCE OF LIGHT AROUND THE ONCOID	

Figure 8. Illustrative scheme summarizing the four main oncoide types and their interpreted genesis conditions separated into three situations: Situation A: containing concave oncoide, type 1, representing concave oncoide, without carbonate production at the base. Situation AB: involves concave oncoide, type 2, representing a transition between A and B situations. Situation B: involves spherical oncoide, types 3 and 4, with concentric lamination and similar carbonate production around the oncoide. Oncoide with A situation genesis likely had *in situ* growth, partially fixed to the substrate. In contrast, oncoide with B situation genesis have grown detached from the bottom substrate, with favorable conditions that allowed similar concentric carbonate production around the oncoide, often subjected to bearing.

The higher plants photosynthesis' influence is negligible due to the oncoide's (cyanobacteria colony) inability to compete with macrophytes (Dandurand *et al.* 1982, Hägele *et al.* 2006). However, in the current tufa-system environment, higher plants influence the phytoherm facies along the rivers (Oste 2017). The abundance of C3 plants also indicates wet conditions, and it holds the $\delta^{13}\text{C}$ around -8.00‰ (Smith *et al.* 2004).

The $\delta^{13}\text{C}$ values between -5.50 to -6.50‰ in oncoide are less negative when compared with values of recent and sub-recent tufas from the Formoso river (-7.00‰ to -9.50‰) (Oste 2017). The less negative data for oncoide indicates a further

specific microbial action (Schidlowski 2000), confirming the lack of macrophytal influence.

Oncoide in Quaternary deposits at Central-West Brasil significance

Active riverine tufas from the Formoso river formed under the same climatic conditions have different facies, interpreted as a consequence of geomorphological features in the environment that controls CO_2 degassing, flow velocity, and consequently the biota development (Oste *et al.* 2021). In summary, there were two predominant features often described in the

literature from the Serra da Bodoquena Region, formed under the actual climatic condition: the riverine and paludal tufas.

Subordinately, the oncoidal floatstones and rudstones were observed in alluvial terraces of the *Formoso River*. Oncoidal facies were described in a riverine environment at the *Formoso River*, cemented in a muddy matrix (Oste *et al.* 2021), and in the *Fazenda São Geraldo's* oncoids underlying unconsolidated micrites (paludal tufas environment) (Utida 2009, Oliveira *et al.*, 2017, Utida *et al.* 2017). We observed oncoids underlying the paludal tufas (massive mudstone Facies), separated by an abrupt and irregular contact. These observations led us to suggest that the genesis of oncoids is not recent and may have occurred before the current time.

The described oncoids possibly had genesis at a time before the establishment of the current tufa precipitation system. In the region's rivers (*Formoso and its tributary*), oncoids in nucleation processes were not observed, and the current absence of oncoids in nucleation may be explained by the fact that oncoids require specific conditions for nucleation. One of the main factors is the absence of macrophytes (higher plants and green algae) and predators such as gastropods (Leinfelder and Hartkopf-Fröder 1990, Hägele *et al.* 2006), both occurring abundantly in the region (Oliveira *et al.* 2017, Utida *et al.* 2017, Oste *et al.* 2021) these aspects can suggest a major climatic change for oncoid nucleation before the establishment of the actual climatic system. The summary of the interpreted evolution of the Formoso River carbonate precipitation system and the ages suggested for oncoid nucleation are shown in Tab. 3.

The age of the rudstone deposits or individual oncoids is still unknown, however, the paludal micrites (Mm) that overlie the oncoidal lenses have shown C^{14} ages of 5,650 to 4,200 to years BP (Sallun Filho *et al.* 2009b) and an estimated depositional rate around ~ 7.5 cm/100 years (Utida 2009). Based on these ^{14}C ages and the thickness (5.0 m) of the deposits, we can infer that a major paludal micrite deposition may have started around 8,500 yr BP, culminating with the lake level fall triggered by a drought period between 8,500 to 4,000 to yr

BP (Absy *et al.* 1991), (Fig. 9) and thus, setting the maximum depositional age of the oncoidal lenses.

Consequently, the oncoid genesis occurred before the major paludal tufa systems establishment and may be related to the end of the Pleistocene and the beginning of the Holocene. Despite the major paludal tufas depositional episode (Boggiani *et al.* 2002, Oliveira *et al.* 2017, Utida *et al.* 2017), relatively small layers continue to deposit in favorable topographic and hydrological conditions (Oste *et al.* 2021). Calcified gastropod shells, macrophyte stalks and calcareous algae increase toward succession, indicating proliferation up the section. The lack of indicative reworking and transport features over long distances indicates that the deposition occurred near the original nucleation site.

We interpreted that oncoid nucleation possibly started after the arboreal pollen decrease in 27,000 yr BP (Ledru 1993) (Fig. 9), since oncoids are unable to compete with macrophyte plants, establishing their minimum nucleation ages where the absence of macrophyte plants and predators such as gastropods, allowing their full development (Hägele *et al.* 2006, Zhang *et al.* 2015, Xiao *et al.* 2020). Recent palinological interpretations in ^{14}C dated samples from the Laguna la Gaiba along the Paraguay River (Pantanal wetlands hydrological linked) interior of Tropical South America, also show colder and drier conditions with an open landscape with smaller trees proliferating and lower lake levels around $\sim 45,000$ and 19,500 yr BP (Whitney *et al.* 2011).

In addition, insolation also affects atmospheric circulation and convective intensity, and consequently the hydrological cycle (Cruz Jr. *et al.* 2005), oxygen isotopic record from radiocarbon on dated lacustrine sediments in Salar de Uyuni, also shows an increase in natural γ -radiation (c.p.s.) around $\sim 20,000$ to 10,000 yr BP, produced by Earth's precessional cycle considering the Tropical South America region (Baker *et al.* 2001). Although we have not seen current oncoid nucleation and growth on actual rivers and a correlation with climatic changes in Central-West Brazil, a more favorable environment

Table 3. Relatively ages interpretations, correlated to environmental conditions.

Epoch	Quaternary Carbonatic Deposits 21°S, 56°W	C^{14} AGE Yr BP (Sallun Filho <i>et al.</i> 2009b)	Relative ages (Interpretative correlation according to Fig. 10)	Palinological record 15° to 25° S, 45° to 60° W (Ledru 1993)	Events
Late Holocene	Riverine tufa (predominance)	2,130 \pm 60; 2,420 \pm 70; 3,410 \pm 70;	—	Evidence of mesophytic, semideciduous forest	Modern Conditions
Middle Holocene	Paludal tufa (predominance)	4,200 \pm 40; 5,650 \pm 50;	—	—	Lake level fall (Absy <i>et al.</i> 1991)
Early Holocene	Alluvial terraces deposition	—	*Around 15,000 to 12,000 yr BP	Low arboreal pollen	Younger Dryas Event (12,900 to 11,700 yr BP)
Late Pleistocene	Spread of oncoids	—	*15,000 to 20,000 yr BP	GAP Sedimentation ceases	Last Glacial Maximum
	Beginning of oncoids nucleation	—	*25,000 yr BP	—	—
	Claystone deposition	—	Before 25,000 yr BP	Drop of arboreal pollen rate	Flooded Planície (Absy <i>et al.</i> 1991)

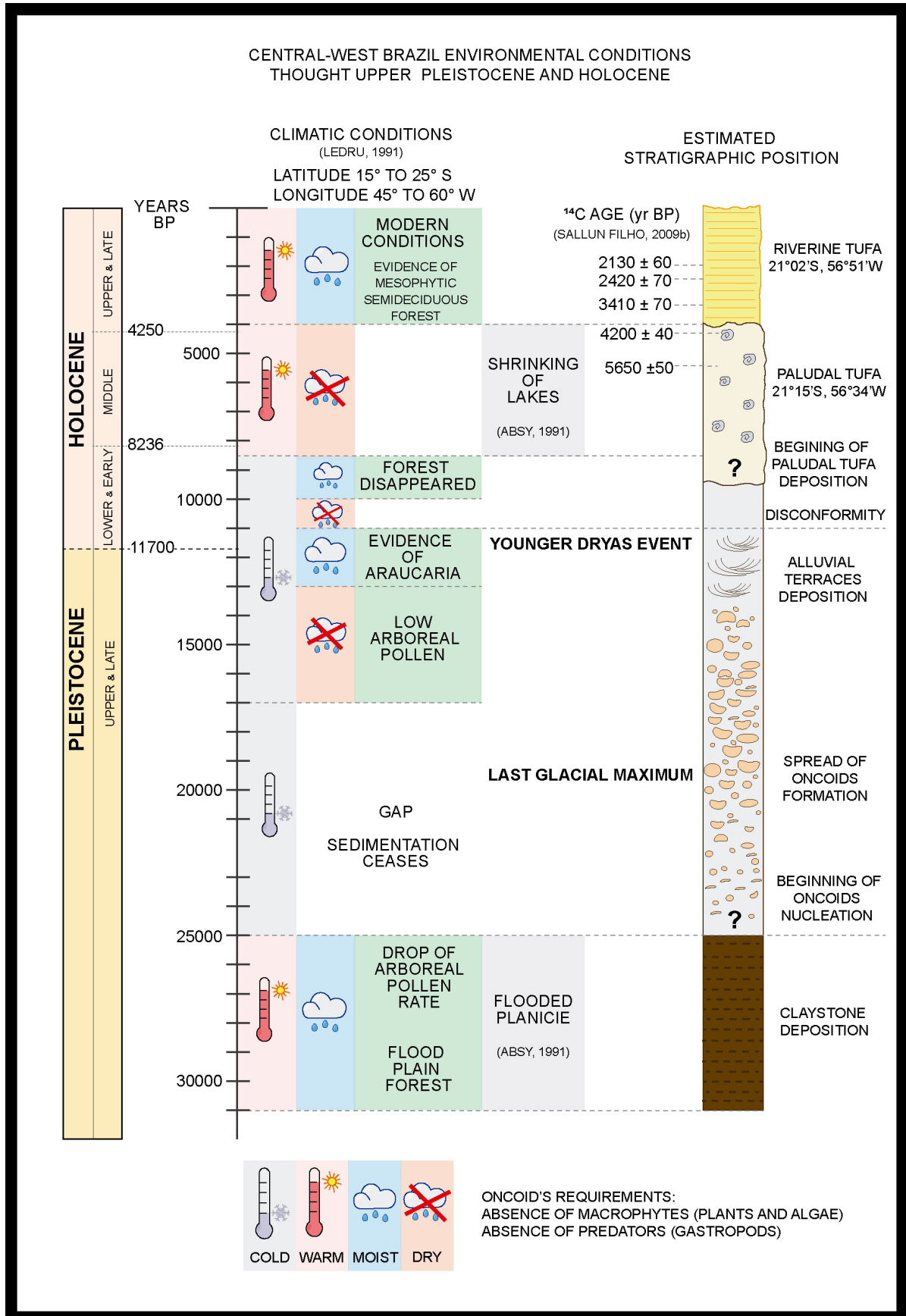


Figure 9. Interpreted climatic and environmental conditions during Upper & Late Pleistocene and Holocene for Midwest Brazil, (Latitude 15° to 25°S, Longitude 45° to 60° W) based on palynological studies (Ledru 1993). The estimated stratigraphic position for oncoidal lenses based on oncoids nucleation and growing requirements (Hägele *et al.* 2006), outcrop features, and previous studies of carbonate deposits in the Serra da Bodoquena Formation, including phytoherm tufa from Aquidabã River (Rio Formoso Member), micrite tufa and Mollusca shells of Fazenda São Geraldo Member (Sallun Filho *et al.* 2009a, Sallun Filho *et al.* 2009b, Oliveira *et al.* 2017, Utida *et al.* 2017). An estimated deposition rate for micrites (7,5 cm for 100 years) allows inferring the beginning of precipitation after the Younger Dryas Event, which culminates with low lake levels suggested by (Absy *et al.* 1991). Oncoids are probably older than the Younger Dryas Event (11,700 to 12,900 years BP). They may represent the depositional gap around 25,000 to 17,000 years BP. The start of oncoids nucleation probably occurred when the arboreal pollen rate decreased 27,000 years ago.

for oncoïd development in the past can be suggested, possibly around ~ 27,000 to 10,000 yr BP.

The Bodoquena Highlands' underground karst system consists of the current tufa system's ion source (Boggiani *et al.* 1993, Oliveira *et al.* 2017), and likely provided the ion source to the oncoïds' genesis in the past. The stratigraphic disposition observed in outcrops and sedimentary structures such as stratification in floatstones and rudstones, and massive structure in mudstone, corroborates the hypothesis of genesis of the oncoïdal facies in a different stage compared to the paludal tufa (Mudstone facies). The oncoïds appear to record a previous climatic system relatively colder and drier.

CONCLUSIONS

These oncoïd occurrences represent the basal interval of the Quaternary deposits of the Serra da Bodoquena downstream plains, and probably occurred under different climatic conditions during the end of the Pleistocene and the beginning of the Holocene. We demonstrated that morphological, chemical, and isotopic aspects of oncoïds coupled with stratigraphic research can provide valuable information concerning nucleation settings and environmental significance. This study interprets that oncoïds grew in a shallow water environment, with a laminar flow incidence, absence of macrophytes and competing organisms.

These oncoïd occurrences represent the basal interval of the Quaternary deposits of the Serra da Bodoquena downstream

plains. Their genesis likely occurred under a different climatic condition during the Upper Pleistocene. The 21°S latitude in Brazil (Tropical South Hemisphere), was probably under colder and drier conditions (Whitney *et al.* 2011, Novello *et al.* 2017, 2019), and oncoïd nucleation possibly occurred under a shallow water body, with a reduced population of competitor organisms such as higher plants (Ledru 1993, Whitney *et al.* 2011), possibly under higher sunlight incidence (Baker *et al.* 2001, Cruz Jr. *et al.* 2005) culminating in favorable conditions for oncoïd-forming cyanobacteria proliferation (Hägele *et al.* 2006, Riding 2006, Zhang *et al.* 2015). Detailed studies with C¹⁴ dating control could bring valuable information concerning the transition between the Pleistocene to the Holocene in Central-West Brazil (Tropical South Hemisphere), constraining the ages and evolution stages of this Quaternary carbonate system and its climatic controls.

ACKNOWLEDGMENTS

We express our gratitude to Petrobras and its partnership with the Universidade Federal do Paraná (UFPR), for providing financial support through the Microbial Project [grant number 23075.120 789/2016-11]. We are very thankful to the São Geraldo Farm help with logistics, the Centro de Microscopia Eletrônica (CME) UFPR, and Centro de Tecnologias Avançadas em Fluorescência (CTAF) UFPR for the petrographic studies.

ARTICLE INFORMATION

Manuscript ID: 20210042. Received on: 06/09/2021. Approved on: 10/08/2021.

A.C.R.: conceptualization, methodology, formal analysis, investigation, writing — original draft; L.R.S.: validation, investigation, writing — review & editing; L.F.C.: conceptualization, investigation, writing — review & editing, supervision; A.M.B.R.: conceptualization, investigation, resources, writing — review & editing, project administration, supervision.

Competing interests: The authors declare no competing interests.

REFERENCES

- Absy M., Cleef A., Van Der Hammen T., Fournier M., Martin L., Servant M., Sifeddine A., Ferreira da Silva M., Soubies F., Suguio K., Turcq B. 1991. Mise en évidence de quatre phases d'ouverture de la forêt dense dans le sud-est de l'Amazonie au cours des 60 000 dernières années. Première comparaison avec d'autres régions tropicales. *Comptes Rendus l'Académie des Sci. 2 Mécanique...*, **312**:673-678.
- Andrews J.E. 2006. Palaeoclimatic records from stable isotopes in riverine tufas: Synthesis and review. *Earth-Science Review*, **75**(1-4):85-104. <https://doi.org/10.1016/j.earscirev.2005.08.002>
- Andrews J.E., Pedley M., Dennis P.F. 2000. Palaeoenvironmental records in Holocene Spanish tufas: A stable isotope approach in search of reliable climatic archives. *Sedimentology*, **47**(5):961-978. <https://doi.org/10.1046/j.1365-3091.2000.00333.x>
- Arp G., Reimer A., Reitner J. 2001a. Photosynthesis-Induced Biofilm Calcification and Calcium Concentrations in Phanerozoic Oceans. *Science*, **292**(5522):1701-1704. <https://doi.org/10.1126/science.1057204>
- Arp G., Wedemeyer N., Reitner J. 2001b. Fluvial tufa formation in a hard-water creek (Deinschwanger Bach, Franconian Alb, Germany). *Facies*, **44**:1-22. <https://doi.org/10.1007/bf02668163>
- Baker P.A., Rigsby C.A., Seltzer G.O., Fritz S.C., Lowenstein T.K., Bacher N.P., Veliz C. 2001. Tropical climate changes at millennial and orbital timescales on the Bolivian Altiplano. *Nature*, **409**:698-701. <https://doi.org/10.1038/35055524>
- Berrendero E., Perona E., Mateo P. 2008. Genetic and morphological characterization of Rivularia and Calothrix (Nostocales, Cyanobacteria) from running water. *International Journal of Systematic and Evolutionary Microbiology*, **58**(2):447-460. <https://doi.org/10.1099/ijs.0.65273-0>
- Boggiani P.C., Coimbra A.M., Gesicki A.L.D., Sial A.N., Ferreira V.P., Ribeiro F.B., Flexor J.-M. 2002. Tufas Calcárias da Serra da Bodoquena, MS. Cachoeiras petrificadas ao longo dos rios. In: Schobbenhaus C., Campos D. de A., Queiroz E.T. de, Manfredo W., Berbert-Born M. (Eds.). *Sítios Geológicos e paleontológicos do Brasil*. Brasília, p. 249-259.
- Boggiani P.C., Fairchild T.R., Coimbra A.M. 1993. O Grupo Corumbá (Neoproterozóico-Cambriano) na região central da Serra da Bodoquena (Faixa Paraguaí), Mato Grosso do Sul. *Revista Brasileira de Geociências*, **23**(3):301-305. <https://doi.org/10.25249/0375-7536.1993233301305>
- Cruz Jr. F.W., Burns S.J., Karmann I., Sharp W.D., Vuille M., Cardoso A.O., Ferrari J.A., Dias P.L.S., Viana Jr. O. 2005. Insolation-driven changes in atmospheric circulation over the past 116,000 years in subtropical Brazil. *Nature*, **434**(7029):63-66. <https://doi.org/10.1038/nature03365>
- Dahanayake K. 1978. Sequential position and environmental significance of different types of oncoïds. *Sedimentary Geology*, **20**:301-316. [https://doi.org/10.1016/0037-0738\(78\)90060-X](https://doi.org/10.1016/0037-0738(78)90060-X)

- Dandurand J.L., Gout R., Hoefs J., Menschel G., Schott J., Usdowski E. 1982. Kinetically controlled variations of major components and carbon and oxygen isotopes in a calcite-precipitating spring. *Chemical Geology*, **36**(3-4):299-315. [https://doi.org/10.1016/0009-2541\(82\)90053-5](https://doi.org/10.1016/0009-2541(82)90053-5)
- Darling W.G. 2004. Hydrological factors in the interpretation of stable isotopic proxy data present and past: a European perspective. *Quaternary Science Review*, **23**(7-8):743-770. <https://doi.org/10.1016/j.quascirev.2003.06.016>
- Decho A.W., Gutierrez T. 2017. Microbial extracellular polymeric substances (EPSs) in ocean systems. *Frontiers in Microbiology*, **8**:1-28. <https://doi.org/10.3389/fmicb.2017.00922>
- Decho A.W., Visscher P.T., Reid R.P. 2005. Production and cycling of natural microbial exopolymers (EPS) within a marine stromatolite. *Palaeogeography, Palaeoclimatology, Palaeoecology*, **219**(1-2):71-86. <https://doi.org/10.1016/j.palaeo.2004.10.015>
- Dunham R.J. 1962. Classification of carbonate rocks according to depositional texture. In: Ham W. (Ed.). *Classification of Carbonate Rocks*. American Association of Petroleum Geologists, p. 108-121.
- Dupraz C., Reid R.P., Braissant O., Decho A.W., Norman R.S., Visscher P.T. 2009. Processes of carbonate precipitation in modern microbial mats. *Earth-Science Review*, **96**(3):141-162. <https://doi.org/10.1016/j.earscirev.2008.10.005>
- Dupraz C., Visscher P.T. 2005. Microbial lithification in marine stromatolites and hypersaline mats. *Trends in Microbiology*, **13**(9):429-438. <https://doi.org/10.1016/j.tim.2005.07.008>
- Embry A., Klovan E. 1971. A late Devonian reef tract on northeastern Banks Island, N.W.T. *Bulletin of Canadian Petroleum Geology*, **19**(4):730-781. <https://doi.org/10.35767/gscpgbull.19.4.730>
- Flügel E. 2010. *Microfacies of Carbonate Rocks*. Cham: Springer. <https://doi.org/10.1007/978-3-642-03796-2>
- Garnett E.R., Andrews J.E., Preece R.C., Dennis P.F. 2006. Late-glacial and early Holocene climate and environment from stable isotopes in Welsh Tufa. *Quaternaire*, **17**(2). <https://doi.org/10.4000/quaternaire.742>
- Gat J.R. 1971. Comments on the stable isotope method in regional groundwater investigations. *Water Resources Research*, **7**(4):980-993. <https://doi.org/10.1029/WR007i004p00980>
- Hägele D., Leinfelder R., Grau J., Burmeister E.G., Struck U. 2006. Oncoids from the river Alz (southern Germany): Tiny ecosystems in a phosphorus-limited environment. *Palaeogeography, Palaeoclimatology, Palaeoecology*, **237**(3-4):378-395. <https://doi.org/10.1016/j.palaeo.2005.12.016>
- Ledru M.-P. 1993. Late quaternary environmental and climatic changes in Central Brazil. *Quaternary Research*, **39**(1):90-98. <https://doi.org/10.1006/qres.1993.1011>
- Leinfelder R.R., Hartkopf-Fröder C. 1990. In situ accretion of concavo-convex lacustrine oncoids ('swallow nests') from the Oligocene of the Mainz Basin, Rhineland, FRG. *Sedimentology*, **37**(2):287-301. <https://doi.org/10.1111/j.1365-3091.1990.tb00960.x>
- Logan B.W., Rezak R., Ginsburg R.N. 1964. Classification and Environmental significance of algal stromatolites. *Journal of Geology*, **72**(1):68-83. <https://doi.org/10.1086/626965>
- Merz M.U.E. 1992. The biology of carbonate precipitation by cyanobacteria. *Facies*, **26**:81-101. <https://doi.org/10.1007/BF02539795>
- Merz-Preiß M., Riding R. 1999. Cyanobacterial tufa calcification in two freshwater streams: Ambient environment, chemical thresholds and biological processes. *Sedimentary Geology*, **126**(1-4):103-124. [https://doi.org/10.1016/S0037-0738\(99\)00035-4](https://doi.org/10.1016/S0037-0738(99)00035-4)
- Nichols G., 2009. Rivers and alluvial fans. In: Nichols, G. (Ed.). *Sedimentology and stratigraphy*. Oxford, Wiley-Blackwell, p. 129-149.
- Novello V.F., Cruz F.W., Mcglue M.M., Wong C.L., Ward B.M., Vuille M., Santos R.A., Jaqueto P., Pessenda L.C.R., Atorre T., Ribeiro L.M.A.L., Karmann I., Barreto E.S., Cheng H., Edwards R.L., Paula M.S., Scholz D. 2019. Vegetation and environmental changes in tropical South America from the last glacial to the Holocene documented by multiple cave sediment proxies. *Earth and Planetary Science Letters*, **524**:115717. <https://doi.org/10.1016/j.epsl.2019.115717>
- Novello V.F., Cruz F.W., Vuille M., Strikis N.M., Edwards R.L., Cheng H., Emerick S., Paula M.S. De, Li X., Barreto E.D.S., Karmann I., Santos R.V. 2017. A high-resolution history of the South American Monsoon from Last Glacial Maximum to the Holocene. *Scientific Reports*, **7**:44267. <https://doi.org/10.1038/srep44267>
- Oliveira E.C. de, Rossetti D.F., Utida G. 2017. Paleoenvironmental evolution of continental carbonates in West-Central Brazil. *Anais da Academia Brasileira de Ciências*, **89**(Suppl. 1):407-429. <https://doi.org/10.1590/0001-3765201720160584>
- Oren A. 2015. Cyanobacteria in hypersaline environments: biodiversity and physiological properties. *Biodiversity and Conservation*, **24**:781-798. <https://doi.org/10.1007/s10531-015-0882-z>
- Oste J. 2017. *Caracterização geoquímica dos depósitos tipo Tufa do Quaternário da Formação Serra da Bodoquena, Membro Rio Formoso-MS*. Curitiba: Universidade Federal do Paraná.
- Oste J.T.F., Rodríguez-Berriguete Á., Dal Bó P.F. 2021. Depositional and environmental controlling factors on the genesis of Quaternary tufa deposits from Bonito region, Central-West Brazil. *Sedimentary Geology*, **413**:105824. <https://doi.org/10.1016/j.sedgeo.2020.105824>
- Pentecost A. 1978. Blue-green algae and freshwater carbonate deposits. *Proceedings of the Royal Society B*, **200**(1138):43-61. <https://doi.org/10.1098/rspb.1978.0004>
- Pentecost A., Spiro B. 1990. Stable carbon and oxygen isotope composition of calcites associated with modern freshwater cyanobacteria and algae. *Geomicrobiology Journal*, **8**(1):17-26. <https://doi.org/10.1080/01490459009377875>
- Pentecost A., Talling J.F. 1987. Growth and calcification of the freshwater cyanobacterium *Rivularia haematites*. *Proceedings of the Royal Society B*, **232**(1266):125-136. <https://doi.org/10.1098/rspb.1987.0064>
- Perona E., Mateo P. 2006. Benthic cyanobacterial assemblages as indicators of nutrient enrichment regimes in a Spanish river. *Acta Hydrochimica et Hydrobiologica*, **34**(1-2):67-72. <https://doi.org/10.1002/ahch.200500611>
- Reviere B. 2002. Divisão Cyanophyta. In: Reviere B. (Ed.). *Biologia e filogenia das algas*. Porto Alegre: Artmed. p. 21-33.
- Riding R. 1975. Girvanella and other algae as depth indicators. *Lethaia*, **8**(2):173-179. <https://doi.org/10.1111/j.1502-3931.1975.tb01310.x>
- Riding R. 2006. Cyanobacterial calcification, carbon dioxide concentrating mechanisms, and Proterozoic-Cambrian changes in atmospheric composition. *Geobiology*, **4**(4):299-316. <https://doi.org/10.1111/j.1472-4669.2006.00087.x>
- Riding R.E., Awramik S.M. 2000. *Microbial sediments*. New York: Springer. <https://doi.org/10.1007/978-3-662-04036-2>
- Sallun Filho W., Karmann I., Boggiani P.C., Petri S., Cristalli P. de S., Utida G. 2009a. A deposição de tufas quaternárias no estado de Mato Grosso do Sul: proposta de definição da formação Serra da Bodoquena. *Geologia USP. Série Científica*, **9**(3):47-60. <https://doi.org/10.5327/z1519-874x2009000300003>
- Sallun Filho W., Karmann I., Sallun A.E.M., Suguio K. 2009b. Quaternary tufa in the Serra da Bodoquena Karst, West-Central Brazil: Evidence of wet period. In: IOP Conference Series: Earth and Environmental Science. *Proceedings ... IOP*, p. 072055. <https://doi.org/10.1088/1755-1307/6/7/072055>
- Schidlowski M. 2000. Carbon isotopes and microbial sediments. In: Riding R.E., Awramik S.M. (Eds.). *Microbial sediments*. New York: Microbial Sediments. Springer, p. 84-95.
- Seltzer G.O., Rodbell D.T., Baker P.A., Fritz S.C., Tapia P.M., Rowe H.D., Dunbar R.B. 2014. Early Warming of Tropical South America at the Last Glacial-Interglacial Transition. *Science*, **296**(5573):1685-1686. <https://doi.org/10.1126/science.12070136>
- Sequero C., Aurell M., Bádenas B. 2020. Oncoïd distribution in the shallow domains of a Kimmeridgian carbonate ramp (Late Jurassic, NE Spain). *Sedimentary Geology*, **398**:105585. <https://doi.org/10.1016/j.sedgeo.2019.105585>
- Shalygin S., Pietrasiak N., Gomez F., Mlewski C., Gerard E., Johansen J.R. 2018. *Rivularia halophila* sp. nov. (Nostocales, Cyanobacteria): the first species of *Rivularia* described with the modern polyphasic approach. *European Journal of Phycology*, **53**(4):537-548. <https://doi.org/10.1080/09670262.2018.1479887>
- Smith J.R., Giegengack R., Schwarcz H.P. 2004. Constraints on Pleistocene pluvial climates through stable-isotope analysis of fossil-spring tufas and associated gastropods, Kharga Oasis, Egypt. *Palaeogeography, Palaeoclimatology, Palaeoecology*, **206**(1-2):157-175. <https://doi.org/10.1016/j.palaeo.2004.01.021>

Utida G. 2009. *Fósseis em micritos Quaternários da Serra da Bodoquena, Bonito-MS e sua aplicação em estudos paleoambientais*. São Paulo: Universidade de São Paulo.

Utida G., Oliveira E.C., Tucker M., Petri S., Boggiani P.C. 2017. Palaeoenvironmental interpretations based on molluscs from mid-Holocene lacustrine limestones, Mato Grosso do Sul, Brazil. *Quaternary International*, **437**(Part A):186-198. <https://doi.org/10.1016/j.quaint.2016.11.007>

Védrine S., Strasser A., Hug W. 2007. Oncoid growth and distribution controlled by sea-level fluctuations and climate (Late Oxfordian, Swiss Jura Mountains). *Facies*, **53**:535-552. <https://doi.org/10.1007/s10347-007-0114-4>

Wang X., Auler A.S., Edwards R.L., Cheng H., Cristalli P.S., Smart P.L., Richards D.A., Shen C.-C. 2004. Wet periods in northeastern Brazil over the past 210 kyr linked to distant climate anomalies. *Nature*, **432**:740-743. <https://doi.org/10.1038/nature03067>

Whitney B.S., Mayle F.E., Punyasena S.W., Fitzpatrick K.A., Burn M.J., Guillen R., Chavez E., Mann D., Pennington R.T., Metcalfe S.E. 2011. A 45 kyr palaeoclimate record from the lowland interior of tropical South America. *Palaeogeography, Palaeoclimatology, Palaeoecology*, **307**(1-4):177-192. <https://doi.org/10.1016/j.palaeo.2011.05.012>

Xiao E., Mei M., Jiang S., Zafar T. 2020. Morphology and features of Cambrian oncoids and responses to palaeogeography of the North China Platform. *Journal of Palaeogeography*, **9**:7. <https://doi.org/10.1186/s42501-020-0055-1>

Zhang W., Shi X., Jiang G., Tang D., Wang X. 2015. Mass-occurrence of oncoids at the Cambrian Series 2-Series 3 transition: Implications for microbial resurgence following an Early Cambrian extinction. *Gondwana Research*, **28**(1):432-450. <https://doi.org/10.1016/j.gr.2014.03.015>

ERRATUM

<https://doi.org/10.1590/2317-4889202220210042erratum>

In the manuscript “Continental freshwater carbonate coated grains: oncoids in Quaternary deposits of the Serra da Bodoquena region, Central-West Brazil”, DOI: 10.1590/2317-4889202220210042, published in the *Braz. J. Geol.*, 52(2):20210042:

Where it reads:

© 2021 The authors. This is an open access article distributed under the terms of the Creative Commons license.

It should read:

© 2022 The authors. This is an open access article distributed under the terms of the Creative Commons license.

Where it reads:

Braz. J. Geol. (2021), 52(2): e20200042

It should read:

Braz. J. Geol. (2022), 52(2): e20200042